Anal. Bioanal. Electrochem., Vol. 10, No. 5, 2018, 631-641

Analytical & Bioanalytical Electrochemistry

Full Paper

Electrochemical Synthesis and Characterization of Ni^{2+} Doped Magnetite Nanoparticles/graphene Oxide Nanocomposite: a Simple and Facile Approach to Prepare Superparamagnetic Composite

Isa Karimzadeh

Department of Physics, Faculty of Science, Central Tehran Branch, Islamic Azad University, Tehran, Iran

*Corresponding Author,

E-Mail: Isa.karimzadeh@gmail.com

Received: 25 February 2018 / Received in revised form: 21 April 2018 / Accepted: 27 April 2018 / Published online: 31 May 2018

Abstract- In this paper, Ni^{2+} doped magnetite nanoparticles/graphene oxide composite are fabricated through an electrochemical synthesis procedure for the first time. The electrosynthesis procedure is based on the electrochemical growth of iron oxide nanoparticles onto the graphene oxide sheets electrophoretically deposited on the cathode electrode. An aqueous solution of iron nitrate nonahydrate (0.3 g), iron chloride tetrahydrate (0.1 g), nickel nitrate hexahydrate (0.1 g) and 0.03 g dispersed graphene oxide was used as the electrosynthesis bath. The X-ray diffraction pattern of the prepared composite revealed that it has magnetite crystal structure. The particle morphology, graphene oxide content and Ni^{2+} cation doping were also confirmed through FE-SEM observations, EDS and FT-IR analyses. The superparamagnetic nature of the fabricated composite was determined from M-H curve and magnetic data obtained by vibrating sample magnetometer (VSM) analysis. The Ni-Fe_3O_4/GO composite showed magnetic data of Ms=47.03 $emug^{-1}$, Mr=0.14 $emug^{-1}$ and Hci=3.76 G. In final, the cathodic electro-synthesis is proposed as a facile electrochemical technique for the fabrication of metal cations doped magnetite NPs/ graphene oxide nanocomposite.

Keywords- Iron oxide, Metal ion doping, Graphene oxide, Electro-chemical synthesis, Nanocomposite

1. INTRODUCTION

Transition metal cations doped magnetic nanoparticles (MNPs) in the form of $M_xFe_{3-x}O_4$ (M=Ni, Co, Mn, Zn, Cr, etc.) are interested to apply in the potential biomedical applications of targeted drug delivery [1], magnetic data storage [2] and magnetic thermos-therapy targeting malignant tumors [3,4]. Furthermore, this form of MNPs have been investigated as the absorbents of contaminated land and water [5,6], catalysis [7], energy storage materials [8-14]. It was found that the magnetic properties of MNPs (i.e. their moment and anisotropy) can be manipulated and optimized by transition metal cations doping, which provides the MNPs properties tuning for different biomedical uses [15]. The magnetic performance of MNPs to transduce external magnetic field energy into a mechanical or thermal response can be exploited for biomedical applications, where many research have performed on developing particles tailored to special specific applications [16-20]. The size, core composition and surface coating of MNPs dedicate their magnetic response to an external magnetic field. Modifying the MNPs composition or doping with metal ions changes the nanoparticles' magnetic anisotropies [21-23] and magnetic moments [11,12]. For example, altering the MNPs magnetic moment affects their contrast ability as MRI agents in magnetic resonance imaging, while their magnetic anisotropy determines whether they are in a superparamagnetic state at physiological media [22,23]. Furthermore, both properties of magnetic anisotropy and magnetic moment affect the heating power of MNPs when exposed to high-frequency oscillating magnetic fields such as those used in magnetic hyperthermia [24]. These effects have revealed the importance of metal cations doping into the iron oxide structure.

Up now, MNPs have been fabricated through various procedures. And, many works have done on SPIONs synthesis via three common methods of co-precipitation, hydrothermal and thermal decomposition, however, the control of the SPIONs size is very vital in order to tune their magnetic properties in the above mentioned fields. In fact, various methods including chemical [25-29], electrochemical [30-40] and mechanical [41,42] have been developed for producing MNPs, however, many of these processes can be expensive and environmentally damaging owing to the use of high temperatures and toxic materials. As an alternative and simple technique, electrodeposition has reported to be facile the preparation method of metal oxide NPs [43-50]. The electrodeposition procedures i.e. both anodic and cathodic ones have been significantly extended in recent years and are the major synthetic route for the production of a variety of inorganic nanomaterials [51]. The various materials including oxides, hydroxides, phosphates, chalcogenides, as well as metals and metal alloys can be electrosynthesized. Here, we applied cathodic electrodeposition for fabrication of Ni^{2+} cations doped MNPs/grapheme composite. It is worth noting that the electrochemical synthesis has not been reported for the fabrication of this type of materials. The magnetic and structural properties of the prepared nan-composite are characterized by XRD, FT-IR, FE-SEM and

VSM analyses. The results confirmed the successful electrochemical fabrication of Ni doped iron oxide NPs/grapheme sheets composite.

2. EXPERIMENTAL PROCEDURE

2.1. Materials

Iron(III) nitrate nonahydrate ($Fe(NO_3)_3$. $9H_2O$, 99.9%), iron(II) chloride tetrahydrate ($FeCl_2 \cdot 4H_2O$, 99%), and nickel chloride hexahydrate ($NiCl_2$.$6H_2O$, 99.5%) were purchased from Sigma Aldrich. Graphene oxide (GO) was provided from IRRIP local company. All materials were used as received and without any purification.

2.2. Electrochemical synthesis of Ni^{2+}-Fe_3O_4/graphene oxide composite

Iron(III) nitrate (0.3 g), iron(II) chloride (0.2 g) and nickel chloride (0.1 g) were dissolved in 100 cc deionized water. The 30 mg graphene oxide was added into this solution and sonicated for 3 h. The prepared solution was used as the electrolyte in the electrodesotion experiments. The stainless-steel and graphite plates were selected to be cathode and anode electrodes, respectively. The electrochemical synthesis processes were done in the constant current (CC) mode with a typical current density of 10 $mAcm^{-2}$. The other deposition parameters i.e. synthesis time and bath temperature were 20 min and 25 ^oC, respectively. After deposition, the form black deposited onto steel electrode was washed several times and then scarped from the electrode. The obtained powder was dried in oven for 2 h in 70 ^oC. In final, the dried powder was named as the final nanocomposite and characterized by various techniques.

2.3. Sample characterization

The FTIR analysis was done at a resolution of 4 cm^{-1} from 400 to 4000 cm^{-1} using a Bruker Vector 22 Fourier transformed infrared spectroscope. A field-emission scanning electron microscopy (FE-SEM, Mira 3-XMU with accelerating voltage of 100 kV) was used to provide the morphological characteristic of the prepared sample. The XRD pattern of the prepared composite was recorded via X-ray diffraction (XRD, Phillips PW-1800). The magnetic data i.e. VSM profile and the related parameters of the prepared powder were provided using vibrating sample magnetometer (VSM, model: Meghnatis Daghigh Kavir Co., Iran).

3. RESULTS AND DISCUSSION

Fig. 1 illustrates XRD pattern of the electro-synthesized powder. Diffraction peaks of our sample can be indexed by the indices of (220), (311), (400), (422), (511), (440), (620), (622)

and (533). No additional peaks are observed. The position or location of all these observed diffraction peaks are related to the iron oxide (Fe_3O_4) with cubic spinel structure with JCPDS number of 01-088-0315. This finding showed that the magnetite phase of iron oxide is electrodeposited in the presence of Ni cation and graphene oxide sheets as additives.

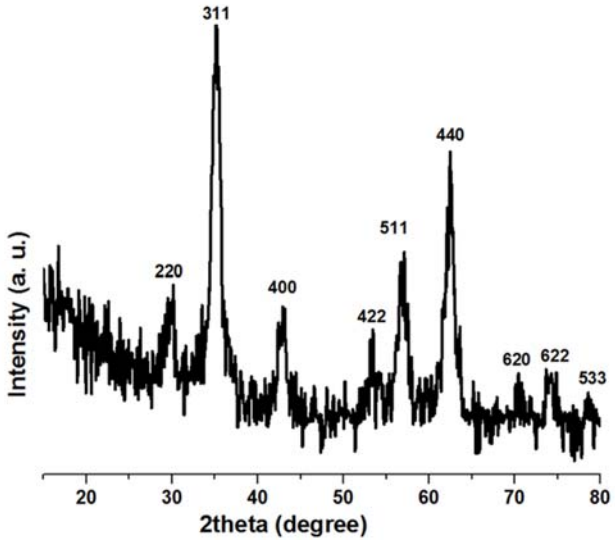

Fig. 1. XRD pattern of the prepared metal ion doped iron oxide/GO composite

Morphological properties (FE-SEM images) and elemental analysis data of the prepared composite (Ni^{2+} doped Fe_3O_4/ GO) are given in Fig. 2. For comparison, the FE-SEM image of the pure Ni^{2+} doped Fe_3O_4 (Fig. 2a) is also provided from previous work of our team [52]. The pure Ni cations doped magnetite has composed of spherical particles with sizes of 10-15 nm. The Ni-Fe_3O_4 particles are collected each other and have some agglomerated nature, as clearly seen in Fig. 2a. As presented in Ref. [52], the Ni doped magnetite has the composition of Fe (62.98 wt%), Ni (10.12 wt%) and O (26.91 wt%), which confirmed the replacement of some Fe^{2+} ions by Ni^{2+}, and is quite in agreement with Fe_3O_4 composition (iron, 72.36 wt% and oxygen, 27.64 wt% [52]). The FE-SEM images of Ni-Fe_3O_4/grapheme sample presents the particle morphology, as observable in Figs. 2a and b. Also, the grapheme layers on both size of particles (i.e. top and down sides) are observed. Some degree of agglomeration was also seen for the magnetite particles. These particles have mean size of 20 nm. The elemental graph provided though Energy-dispersive X-ray spectroscopy (EDAX) from the Fig. 2c is shown in Fig. 2d. In this graph, the presence of Fe, Ni, C and O elements is clearly seen. The amounts of these elements are also given in (Fig. 2e). As listed in Fig. 2e, the composite sample contains elemental composition of Fe (43.22%), and Ni (7.07%), O (33.35%) and carbon (16.36%). The magnetite composition of the prepared sample is evidenced from the Fe and O amounts. The Ni presence provides the proper evidence that the prepared composite

has Ni doped magnetite composition. The GO part of the electrosynthesized sample is also confirmed via C content in the EDS data (Fig. 2e). These results indicated the facile preparation of Ni doped Fe_3O_4 NPs/graphene oxide sheets composite through electrochemical synthesis.

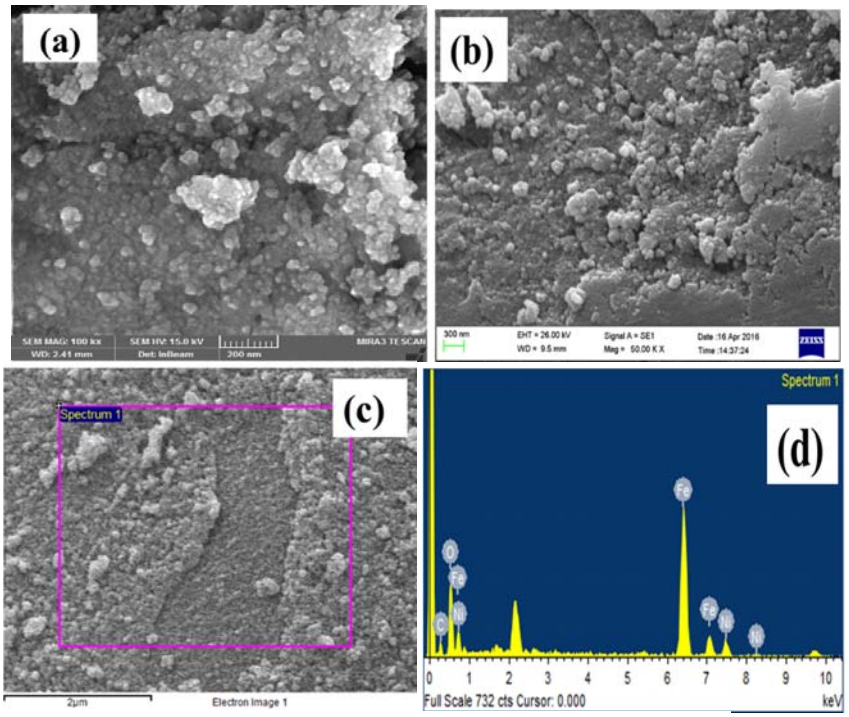

(e)

Element	Weight%	Atomic%
C	16.36	31.38
O	33.35	48.01
Fe	43.22	17.83
Ni	7.07	2.78
Totals	100.00	

Fig. 2. FE-SEM images of (a) pure Ni doped iron oxide and (b,c) its composite with GO, and (d) EDS graph and (e) the elemental percentages in the composition of prepared sample

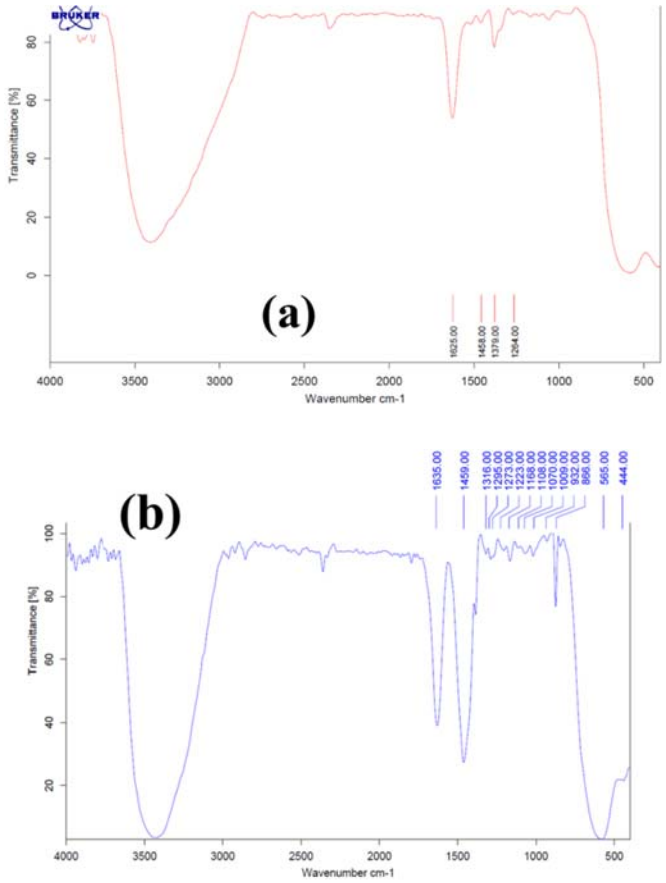

Fig. 3. IR spectra of the synthesized (a) pure Ni doped iron oxide and (b) its composite with GO

IR spectra of the prepared iron oxide samples are presented in Fig. 3. For both samples, the two bands at 634 and 565 cm^{-1} for Fe_3O_4 nanoparticles result from split of the band at 545 cm^{-1} and shift to higher wavenumbers [54]. In fact, these absorptions are due to the Fe-O-Fe and/or Fe-O-Ni vibrations in tetrahedral sites and the next one at 444 cm^{-1} is from the Fe-O-Fe vibration at octahedral sites in Fe_3O_4 crystal structure [11-13]. Notably, the band at 444 cm^{-1} for Fe_3O_4 results from the shifting of the 370 cm^{-1} band to a higher wavenumber [54]. There are some extra peaks in both spectra presented in Fig. 3. For the pure Ni-Fe_3O_4 sample, the absorption peaks at 1626 cm^{-1} is related to the water molecules and OH groups attached into the magnetite NPs [26]. The IR peaks at 1458, 1379 and 1284 cm^{-1} are due to the nitrate and carbonate ions intercalated into the MNPs [31-33]. These IR bands of GO/MNPs sample are as follows; strong absorption bands between 3300 and 3500 cm^{-1} were due to O–H stretching vibration [54], the IR peaks presented by graphene oxide are between 1300 and 1100 cm^{-1}, which are connected to the stretching of phenyl-carbonyl C–C bonds [54,55]. It was reported that the peaks at about 3432 and 1711 cm^{-1} are related to –OH and C=O bands, respectively. Upon reduction of graphene oxide to graphene, the C=O band disappears and

new bands at 2928 and 2865 cm^{-1} arise representing the C-H stretch vibrations of the methylene group [57]. In our magnetite/rGO, there is no IR peak at about 1700 cm^{-1}, indicating the reduction of GO into rGO during the basic electrosynthesis of magnetite on the cathode electrode. Furthermore, the presence of the 2905 and 2854 cm^{-1} are due to the C-H bonds of -CH_3 group. Notably, functionalized graphene displays a peak at 1731 cm^{-1} characteristic band for C=O stretch of the COOH group, where the strong and broad band at 3412 cm^{-1} provides clear evidence for presence of carboxylic functional group [56-58]. The characteristic band of the carboxyl group in GO appears at 3430 cm^{-1} (O–H stretching vibration), 1635 cm^{-1} (skeletal vibrations from un-oxidized graphitic domains [58]), 1354 cm^{-1} (O–H deformations in the C–OH groups), 866 cm^{-1} (C–C stretching vibrations) [57,58], 1223 cm^{-1} (C–OH stretching vibration), and 1070 cm^{-1} (C–O stretching vibration in C–O–C in epoxide), peaks at ~1525 cm^{-1} (C=O stretching vibration) and ~1459 cm^{-1} (C-OH stretching vibration), the bands at 1459 cm^{-1}, 1316 cm^{-1}, 1295 cm^{-1} and 1168 cm^{-1} are due to the -CH_2 and C-H stretching and waging vibration modes [37,58]. The IR findings are completely provided the chemical composition of Ni doped Fe_3O_4/reduced graphene oxide composite for the electrosynthesized sample.

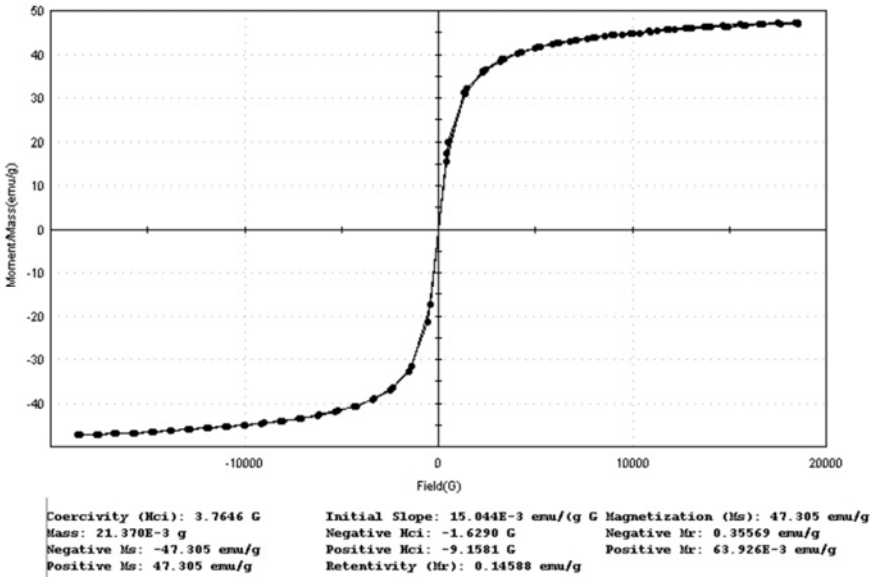

Fig. 4. Magnetization curve obtained by vibrating sample magnetometer (VSM) analysis at room temperature

The magnetic properties of the prepared composite was examined through investigated through vibrating sample magnetometer (VSM) with recording M-H curve at the applied field of -2000 to 2000Oe, which is presented in Fig. 4. Also, the values of saturation magnetization (*Ms*), remnant magnetization (*Mr*) and coercivity (*Hci*) of our sample were specified and

shown in inset of Fig. 4. The M-H profile of our sample revealed that the powder composed of Ni-Fe_3O_4 and graphene oxide exhibits the superparamagnetic nature. The *Ms*, *Mr* and *Hci* values of Ni-Fe_3O_4/GO are 47.03 $emug^{-1}$, 0.145 $emug^{-1}$ and 3.76 G, respectively. These data further proved the superparamagnetic nature of the prepared composite. These data was compared with those of pure/undoped Fe_3O_4, Ni cations doped Fe_3O_4 and its composite with graphene oxide. And the magnetic data of these three samples are listed in Table 1.

Table 1. Comparison between the reported magnetic data of undoped magnetite NPs, Ni^{2+} doped MNPs and its GO composite

Sample name	**Ms(emu/)g**	**Coercivity (Hci)G**	**Positive (Hci) G**	**Negative (Hci)** G	**Negative Mr(emu/g)**	**Positive Mr(emu/g)**	**Retentivity Mr(emu/g)**	**Ref.**
Undoped	72.96	14.6	-41.87	-12.66	0.83	2.73	0.95	[59,60]
Ni-	41.47	4.34	21.39	12.71	-0.82	-0.48	0.17	[52]
Ni-MNPs/	47.03	3.76	-9.15	-1.62	0.35	0.06	0.14	This work

Comparison of the saturation magnetization of theses iron oxide samples showed that the *Ms* value of iron oxide is reduced with Ni^{2+} doping. This is may be due to the low magnetic nature of Ni as compared with iron. However, the *Ms* value of iron oxide composite is bigger than that of pure Ni-MNPs, which is due to the large particle size of electrosynthesized iron oxide NPs in the presence of GO sheets (as seen in Fig. 2). The magnetic retentivity (*Mr*) data for undoped MNPs, Ni-MNPs and Ni-MNPs/GO sample are 0.95 emu/g, 0.17 emu/g and 0.14 emu/g, respectively (Table 1). These *Mr* values indicate that metal ion doped iron oxide NPs show lower Mr and their magnetic response vs. magnetic field is better as compared the M-H behavior of undoped MNPs. Furthermore, with GO composting, the Mr value is shifted to lower values (i.e. 0.172 emu/g → 0.145 emu/g). The same trend is also observed for the coercivity of these samples i.e. *Hci*(Ni-MNPs/GO)<*Hci*(Ni-MNPs)<*Hci*(undoped MNPs). It is worth noting that the coercivity of iron oxide is lowered as a result of its compositing with GO (i.e. 4.34 G → 3.67 G). These better magnetic characters of Ni-MNPs/GO sample (i.e. low remnant magnetization and coercivity) may be connected to the not-agglomerated morphology (Fig. 2) and single-domain behavior of the Ni-MNPs electrodeposited onto graphene oxide sheets.

4. CONCLUSION

In the current study, an electrochemical method was for the first time developed for preparation of superparamagnetic metal cations doped magnetite nanoparticles composited

with reduced graphene oxide. This nanocomposite was cathodically deposited onto steel cathode by applying the *dc* mode in the simple two-electrode system. The deposition product was Ni^{2+} doped Fe_3O_4 nanoparticles (with 20 nm in sizes) grown onto reduced graphene oxide sheets as confirmed by results obtained through XRD, FT-IT, EDS and FE-SEM analyses. An improvement in the superparamagnetic behavior of iron oxide NPs was observed as results of its doping with metal cations and compositing with graphene oxide.

REFERENCES

[1] C. Alexiou, W. Arnold, R. J. Klein, F. G. Parak, P. Hulin, C. Bergemann, W. Erhardt, S. Wagenpfeil, and A. S. Lübbe, Cancer Res. 60 (2000) 6641.
[2] H. Zeng, C. T. Black, R. L. Sandstrom, P. M. Rice, C. B. Murray, and S. H. Sun, Phys. Rev. B 73 (2006) 020402.
[3] M. Johannsen, Int. J. Hyperthermia 21 (2005) 637.
[4] G. F. Goya, V. Grazu, and M. R. Ibarra, Curr. Nanosci. 4 (2008) 1.
[5] R. S. Cutting, Environ. Sci. Technol. 44 (2010) 2577.
[6] V. Hencl, P. Mucha, A. Orlikova, and D. Leskova, Water Res. 29 (1995) 383.
[7] V. Polshettiwar, R. Luque, A. Fihri, H. Zhu, M. Bouhrara, and J. M. Basset, Chem. Rev. 111 (2011) 3036.
[8] M. Aghazadeh, I. Karimzadeh, and M. R. Ganjali, J. Mater. Sci. 28 (2017) 13532.
[9] M. Aghazadeh, and M. R. Ganjali, J. Mater. Sci. 53 (2018) 295.
[10] M. Aghazadeh, I. Karimzadeh, and M. R. Ganjali, J. Electronic Mater. 47 (2018) 3026.
[11] M. Aghazadeh, and M. R. Ganjali, Ceram. Int. 44 (2018) 520.
[12] M. Aghazadeh, and M. R. Ganjali, J. Mater. Sci.: Mater. Electron. 29 (2018) 2291.
[13] M. Aghazadeh, I. Karimzadeh, M.R. Ganjali, and A. Behzad, J. Mater. Sci. 28 (2017) 18121.
[14] M. Aghazadeh, Mater. Lett. 211 (2018) 225.
[15] S. Moise, E. Céspedes, D. Soukup, J. M. Byrne, A. J. El Haj, and N. D. Telling, Scientific Reports 7 (2017) 39922.
[16] Q. A. Pankhurst, N. T. K. Thanh, S. K. Jones, and J. Dobson, J. Phys. D-Appl. Phys. 42 (2009) 224001.
[17] L. Mohammed, H. G. Goma, D. Rag, and J. Zhu, Particuology 30 (2017) 1.
[18] R. Serrano García, S. Stafford, and Y. K. Gun'ko, Appl. Sci. 8 (2018) 172.
[19] T. Kang, F. Li, S. Baik, Wei Shao, D. Ling, and T. Hyeon, Biomater. 136 (2017) 98.
[20] V. Fernandes, C. A. Francesko, C. Ribeiro, M. Bañobre-López, P. Martins, and S. Lanceros-Mendez, Adv. Healthcare Mater. 7 (2018) 1700845.
[21] Y. W. Jun, J. W. Seo, and A. Cheon, Accounts Chem. Res. 41 (2008) 179.
[22] S. Staniland, W. Williams, N. Telling, G. Van Der Laan, A. Harrison, and B. Ward, Nat. Nanotechnol. 3 (2008) 158.

[23] E. Fantechi, C. Innocenti, M. Albino, E. Lottini, and C. Sangregorio, J. Magn. Magn. Mater. 380 (2015) 371.
[24] M. Angelakeris, Biochim. Biophys. Acta 1861 (2017) 1642.
[25] J. Liang, Y. Wu, C. Liu, Y. C. Cao, and Y. Lin, Sens. Actuators B 241 (2017) 758.
[26] M. Aghazadeh, R. Ahmadi, D. Gharailou, M. R. Ganjali, and P. Norouzi, J. Mater. Sci. 27 (2016) 8623.
[27] T. Iwasaki, N. Mizutani, S. Watano, T. Yanagida, and T. Kawai, J. Experimental Nanosci. 5 (2010) 251
[28] C. Ravikumar, and R. Bandyopadhyaya, J. Phys. Chem. C 115 (2011) 1380.
[29] A. H. M. Yusoff, M. Nabil Salimi, and M. Faizal Jamlos, AIP Conference Proceedings 1835 (2017) 020010.
[30] M. Aghazadeh, I. Karimzadeh, and M. R. Ganjali, Mater. Lett. 209 (2017) 450.
[31] M. Aghazadeh, and I. Karimzadeh, Curr. Nanosci. 14 (2018) 42.
[32] I. Karimzadeh, M. Aghazadeh, M. R. Ganjali, P. Norouzi, T. Doroudi, and P. H. Kolivand, Mater. Lett. 189 (2017) 290.
[33] I. Karimzadeh, M. Aghazadeh, M. R. Ganjali, and T. Dourudi, Curr. Nanosci. 13 (2017) 167.
[34] I. Karimzadeh, M. Aghazadeh, T. Doroudi, M. R. Ganjali, P. H. Kolivand, and D. Gharailou, Curr. Nanosci. 13 (2017) 274.
[35] M. Aghazadeh, I. Karimzadeh, M. R. Ganjali, and M. Mohebi Morad, Mater. Lett. 196 (2017) 392.
[36] I. Karimzadeh, H. Rezagolipour Dizaji, and M. Aghazadeh, J. Magn. Magn. Mater. 416 (2016) 81.
[37] I. Karimzadeh, M. Aghazadeh, M. R. Ganjali, P. Norouzi, S. Shirvani-Arani, T. Doroudi, P.H. kolivand, S. A. Marashi, and D. Gharailou, Mater. Lett. 179 (2016) 5.
[38] I. Karimzadeh, H. Rezagolipour Dizaji, and M. Aghazadeh, Mater. Res. Express. 3 (2016) 095022.
[39] M. Aghazadeh, A. Bahrami-Samani, D. Gharailou, M. Ghannadi Maragheh, and M. R. Ganjali, J. Mater. Sci. 27 (2016) 11192.
[40] M. Aghazadeh, and M. R. Ganjali, J. Mater. Sci. 28 (2017) 8144.
[41] M. M. Can, S. Ozcan, A. Ceylan, and T. Firat, Mater. Sci. Engin. B 172 (2010) 72.
[42] J. F.de Carvalho, S. N. de Medeiros, M. A. Morales, A. L. Dantasd, and A. S. Carriço, Appl. Surf. Sci. 275 (2013) 84.
[43] M. Aghazadeh, A. A. M. Barmi, H. M. Shiri, and S. Sedaghat, Ceram. Int. 39 (2013) 1045.
[44] M. Aghazadeh, M. G. Maragheh, M. R. Ganjali, and P. Norouzi, RSC Adv. 6 (2016) 10442
[45] M. Aghazadeh, A. A. M. Barmi, and M. Hosseinifard, Mater. Lett. 73 (2012) 28.

[46] M. Aghazadeh, and S. Dalvand, J. Electrochem. Soc. 161 (2014) D18.
[47] M. Aghazadeh, M. R. Ganjali, and P. Norouzi, J. Mater. Sci. 27 (2016) 7707.
[48] M. Aghazadeh, M. Asadi, M. R. Ganjali, P. Norouzi, B. Sabour, and M. Emamalizadeh, Thin Solid Films 634 (2017) 24.
[49] M. Aghazadeh, M. R. Ganjali, and P. Norouzi, Mater. Res. Express. 3 (2016) 055013.
[50] M. Aghazadeh, T. Yousefi, and M. Ghaemi, J. Rare. Earths 30 (2012) 236.
[51] G. V. Govindaraju, G. P. Wheeler, D. Lee, and K. S. Choi, Chem. Mater. 29 (2017) 355.
[52] M. Aghazadeh, and M. R. Ganjali, J. Mater. Sci. 29 (2018) 4981.
[53] J. L. Zhang, R. S. Srivastava, and R. D. K. Misra, Langmuir 23 (2007) 6342.
[54] M. Yamaura, R. L. Camilo, L. C. Sampaio, M. A. Macedo, M. Nakamura, and H. E. Toma, J. Magn. Magn. Mater. 279 (2004) 210.
[55] N. Gan, J. Zhang, S. Lin, N. Long, T. Li, and Y. Cao, Mater. 7 (2014) 6028.
[56] M. Naebe, J. Wang, A. Amini, H. Khayyam, N. Hameed, L. Hua Li, Y. Chen, and B. Fox, Scientific Reports 4 (2014) 4375.
[57] Y. Tang, F. Huang, W. Zhao, Z. Liu, and D. Wan, J. Mater. Chem. 22 (2012) 11257.
[58] A. Omidvar, M. R. RashidianVaziri, B. Jaleh, N. Partovi Shabestari, and M. Noroozi, Chin. Phys. B 25 (2016) 118102.
[59] M. Aghazadeh, I. Karimzadeh, and M. R. Ganjali, J. Mater. Sci. 28 (2017) 19061.
[60] M. Aghazadeh, J. Mater. Sci. 28 (2017) 18755.